ISSN 2354-9114 (online), ISSN 0024-9521 (print)
Indonesian Journal of GeographyVol 56, No 1 (2024): 138-148
DOI: 10.22146/ijg.93456 website: https://jurnal.ugm.ac.id/ijg

INDONESIAN JOURNAL OF GEOGRAPHY

RESEARCH ARTICLE

Exploring Aceh Fault Zone for Slip Rates and Paleoseismic Trenching Potential along Sumatran Fault

Gayatri Indah Marliyani[1], Yann Klinger[2], Aulia Kurnia Hady[3], Agung Setianto[1], Hurien Helmi[4], Telly Kurniawan[5], Retno Agung Prasetyo Kambali[5], Zulham Sugito[5], Abdi Jihad[5], Yosi Setiawan[5], Andi Azhar Rusdin[5], Supriyanto Rohadi[5], Rahmat Triyono[5], Dwikorita Karnawati[1,5]

[1]Geological Engineering Department, Faculty of Engineering, Universitas Gadjah Mada, Jl Grafika No 2, Yogyakarta, Indonesia
[2]Tectonics Laboratory, Institut de Physique du Globe de Paris - Université de Paris Cité, 1 Rue Jussieu, Paris, France
[3]Department of Energy and Mineral Resources of NAD Province, l. Teuku Nyak Arief No.195, Kota Banda Aceh, Indonesia
[4]Geological Engineering Department, Faculty of Engineering and Planning, Institut Teknologi Nasional Yogyakarta, Jl. Babarsari, Tambak Bayan, Caturtunggal, Yogyakarta, Indonesia
[5]Meteorology, Climatology, and Geophysical Agency of Indonesia, Jl. Angkasa I No. 2 Kemayoran, Jakarta Pusat, Indonesia

Received : 2024-01-23
Revised: 2024-02-01
Publish: 2024-04-30

Keywords: Aceh Fault; offset channels; paleoseismology; Sumatran Fault

Correspondent email: gayatri.marliyani@ugm.ac.id

Abstrac. We conducted a study on the Aceh Fault, an active right-lateral strike-slip fault in northern Sumatra, Indonesia. Despite its seismic hazard potential, the slip characteristics of this fault are not well-understood. Using a combination of remote sensing and field methods, we mapped the distribution of displacement recorded by offset channels along the fault. Our goal is to identify evidence of past surface rupture, characterize their tectonic geomorphology setting, and assess their potentials as slip-rate and paleoseismic sites. The documented right-lateral displacements of channels and ridges from 35 observation points are mostly in the order of magnitude of hundreds of meters, with only a few sites exhibiting meter-scale measurable offsets. Our results provide important first-order data that can be used to locate sites suitable for paleoseismic trenching or offset investigations. This information will support the development of a maximum magnitude and earthquake recurrence model of the fault, which are crucial for seismic hazard analysis in the region.

1. Introduction

Understanding the stress accumulation and release pattern along a fault is important to assess its seismic hazard. For instance, deciphering the mechanism of deformation, whether it is released seismically or through aseismic creep, is crucial to evaluate the potential for hazard. As indicated by various active fault investigations, estimation of the magnitude of past earthquakes can be modeled using distribution of surface displacement along a fault (Sieh, 1978; Lindvall et al., 1989; Rockwell et al, 1990; McGill and Sieh, 1991; Wells and Copersmith, 1994; McGill and Rubin, 1999; Kondo et al., 2005; Zielke et al., 2010). The surface displacement associated with past earthquake ruptures can be recognize through detailed mapping of small-scale offsets of geomorphic features such as rills, channels, hills, and alluvial bars (i.e Klinger et al., 2011). Distributions of these features may reveal the slip distribution of past earthquakes as they can be preserved over a century or more. However, preservation of these features requires certain conditions. Reitman et al. (2023) suggest that changes in climate conditions, particularly variations in rainfall and temperature, can impact the activity and visible characteristics of strike slip faults, shedding light on the complex interplay between geology and climate. So far, this type of study has been mainly conducted in arid-semi arid environment, with only a few study cases in moderate to humid areas (Beaupretre et al., 2012; De Pascale et al., 2014; Langridge et al., 2014; Jayangondaperumal et al 2018).

The Aceh Fault in western Indonesia is the northernmost section of the Great Sumatran Fault (GSF, Figure 1). There is no record of large earthquake along this fault in the past 170 years (Sieh and Natawidjaja, 2000; Tabei et al., 2017; Irsyam et al., 2020). The geomorphic expression of the Aceh Fault, however, corresponds to a prominent fault scarp in the topography, indicating that ground-rupturing earthquakes have occurred in the past (Figure 2). Even though there have been no large damaging earthquakes along this fault in historical records, moderate-sized earthquake events are frequent (yellow stars, Figure 2), indicating that the fault is active. These events prompt a reevaluation of the role of the Aceh Fault in accommodating the slip of the GSF and its potential hazards for the ~546 thousands people living along the fault.

Despite Aceh Fault's recent seismic activities, the segmentation and slip characteristics of this fault, and of the GSF in general, are poorly constrained. The limited publications

available regarding the geological slip rate estimate along the Aceh Fault (and GSF), can be attributed to dense vegetation and challenging accessibility. Some frequently cited slip rate of the northern GSF is at of 38 mm/year. This rate was suggested by McCaffrey et al. (2000), who employed geodetic method and adopted a simple model by Fitch [1972]. Fitch (1972) model proposes that the forearc plate, delimited by the trench and transcurrent fault, behaves rigidly, allowing the inference of long-term average slip rates from fault geometry, slip vectors, and plate motion vectors. Meanwhile, the AGNeSS GPS array measured right-lateral elastic strain accumulation rates, records 20±6 mm/yr across the Aceh Fault from 2005 to 2010 [Ito et al., 2012]. The discrepancy exceeding 10 mm between modeled geological and geodetic slip rate estimates emphasizes the necessity of supplying a reliable geological slip rate data along the fault.

We mapped the lateral displacement recorded by many geomorphological features along the Aceh Fault, using an 8-m resolution digital elevation model of DEMNAS (freely downloaded through https://tanahair.indonesia.go.id/demnas/#/) for the entire study area complemented by sub-meters resolution DEM constructed from aerial photography in some selected sites. Using these datasets, we mapped the geomorphic fault zone, where we could recognize zone of lateral offsets across the fault. The goal is to identify evidence of past surface ruptures, characterize their tectonic geomorphology setting, and to assess their potential as slip-rate and paleoseismic sites.

Visible offset does not always guaranty that we are locating exactly the zone of coseismic deformation, as post-earthquake landscape evolution could have modified the landscape by widening the geomorphic fault zone and obliterate some deformation pattern (Reitman et al., 2019; Reitman et al., 2023). However, we used the distribution of these data as an initial assessment of the fault zone to locate prospective areas for more detailed study.

Deformation in the western part of Indonesia is dominated by oblique subduction of the Indo-Australian oceanic plate beneath the Eurasian continental plate with a rate of ~70 mm/year (McCaffrey, 2009; Tregoning et al., 2002). This subduction zone is known as the Sunda subduction zone. The horizontal slip vector of the highly oblique convergence is largely accommodated by the right-lateral motion of the GSF system, which runs through the entire Sumatra Island, roughly parallel to the trench direction (McCaffrey, 2000; Genrich et al. 2000). If we consider the GSF as the sole fault system accommodating the trench-parallel slip vector of the Sunda subduction in Sumatra, this would imply a maximum slip-rate of 40-60 mm/year, establishing the fault as one of the fastest faults in the world (Jarrard, 1986; McCaffrey, 1992). However, an offshore seismic survey revealed another trench-parallel strike-slip fault system in the forearc, namely the Mentawai Fault (Diament et al., 1992) which connects to the GSF through the Batee Fault (Figure 1). It is likely that both the Mentawai and the Batee Faults are accommodating some parts of the shear component of the convergence, although the slip distribution between them is still unclear as the Mentawai Fault slip-rate is unknown (Bellier and Sebrier, 1995; Bellier et al., 1997).

The geological and geophysical observations indicate that the GSF is active (Sieh and Natawidjaja, 2000; Bellier et al., 1997; Bellier and Sebrier, 1995; Bennet et al., 1981). The northwest trending Aceh Fault represents the northernmost section of the GSF. McCaffery et al. (2000) proposed a geodetic slip rate of 38 mm/year. A GPS campaign conducted by Genrich et al. (2000) estimated the slip-rate of the Aceh Fault to be at ~23-27 mm/year. Meanwhile, Ito et al. (2012) based on continuous and campaign GPS network inferred a slip rate of 20 ± 6 mm/year across the Aceh fault.

The total length of the Aceh Fault is 250 km. It was initially considered as a single fault section (Sieh and Natawidjaja, 2000). This would imply a maximum earthquake magnitude of up to Mw7.9, based on the empirical relationship of Wells and Coppersmith (1994), assuming a fault dip of 90° and a seismogenic depth of 20 km. In the National Earthquake Hazard Map of Indonesia (Pusat Studi Gempa Nasional, 2017) the Aceh Fault is divided into three segments: Aceh North, Aceh Central, and Aceh South, with estimated maximum magnitude respectively of M6.7, 7.2 and 7.6. Hady and Marliyani (2020) proposed another segmentation model based on the fault discontinuities where they divided the Aceh Fault into 7 new fault segments ranging from 15.7 – 50 km with an estimated earthquake magnitude ranging between M6.5 and 7.2.

The Aceh Fault is indicated by a prominent straight fault scarps in the topography. It is separated from Tripa fault segment in the southeast by a 9 km wide restraining bend (Sieh and Natawidjaja, 2000) (Figure 1). In the northwestern part, the Aceh Fault passes through the low relief region of Banda Aceh, continues offshore, and merges with the Andaman Nicobar Fault (Curray et al., 1979; Singh et al., 2013).

2. Methods

The Aceh Fault is dominated by right-lateral displacement. For this study, we only measured the lateral offset and disregarded displacement caused by the vertical slip component of the fault. We analyzed the 8-m resolution DEM data from DEMNAS (freely downloaded through https://tanahair.indonesia.go.id/demnas/#/) for the entire area and our newly acquired 15-cm resolution DEM constructed from UAV drone aerial photos for selected sites. We mapped geomorphic features along the faults that may record lateral displacements, such as channels and ridges. We determine the piercing points manually, by observing the characteristics of the river channel and hillslope morphology. We matched similar features across the fault, such as channel margins, thalwegs, and ridge-crests and measured the along-strike separation of these features by using manual back-slip methods (Zielke et al., 2015).

Because of Sumatra's humid condition, finding well-preserved geomorphic features is challenging. In areas where lateral separation of geomorphic features is observed, but the piercing point does not rest onto the fault, we projected the feature to the fault and measured the slip along the fault-strike.

Further, we ranked the data following quality assessment of offset channels developed by Salisbury et al. (2015). The assessment is mostly based on the channel obliquity relative to the fault trace, fault zone width, and the distance of the piercing points to the fault. While the criteria were initially designed to assess observations in arid and semi-arid environments, we believe that the evaluation's underlying principles are still applicable as a first-order assessment for observations in tropical regions. We determined the extent of the fault zone by outlining the width of the fault scarp and identifying any visible signs of secondary faulting. However, we should note that our definition of the fault zone width may not directly represent zone of coseismic deformation.

In locating sites for paleoseismic and slip-rate studies, finding dateable material is crucial to quantify the fault's rate of displacement. To achieve this, we estimated the lithology based on surface characteristics and double-checked with available geological maps. Additionally, we assessed the availability of dateable material by considering the geomorphological configuration of the site. Accessibility is also taken into account during this evaluation. All of this information collectively assists us in evaluating prospective sites for paleoseismic and slip-rate studies.

3. Results and Discussion

Detailed map of the Aceh Fault zone is presented in Figure 2. We delineated the fault scarp and selected the most recently formed scarp, identified by its relatively sharpness and continuous topographic signature. We prioritized the most prominent scarp for our observations and chose sites along these faults. We identified a total of 48 fault-offset geomorphic features along the Aceh Fault zone, while we were able to measure the lateral offset on 35 features. Map of the locations of the observation sites is shown in Figure 2. The description of these sites is presented by fault sections, arranged by sequence numbers (1-48), starting at Beutong section in the southeast, and ending at Pulo Aceh in the northwest (Figure 3-10).

The documented right-lateral displacements of channels and ridges are dominated by hundreds of meters offset, and only a few sites exhibit meter-scale measurable offsets. The result of the offset measurements is presented in Table 1 and their spatial distribution and amplitude frequency is presented in Figure 11. The geomorphic offset observed here is considered a record of the repetition of earthquakes on a localized fault plane (cumulative offsets). Measuring the displacement can be linked to the timing of these events to determine the fault slip rate. The calculated cumulative offsets have a large variation and a high measurement uncertainty. Most of the topographic data used here, which are derived from the 8m DEM, are not accurate enough to capture meter-scale displacements. Additionally, as emphasized by Reitman et al. (2023), the preservation of fault offset can also be complicated by changes in climate conditions, including variations in rainfall and temperature. Considering the tropical conditions of the Sumatra region, where dense vegetation cover is common and anthropogenic modifications can be drastic due to rice paddies, preserving small offsets, especially if they are not recent, is challenging.

The smallest identified offset, 12.7 m, is recorded along the Geumpang section. The largest offsets we measured, ~2300 m, are located along Kuala Tripa and Jantho sections. The most frequently measured offsets clustered around 300, 185, and 130 m (Figure 11). Our observations indicate that fault sections with valley-bound topography, such as Geumpang and Jantho area, have more observation points compared to other faults bordered by mountainous topography on both sides, such as along the Beutong and Kuala Tripa regions.

3.1. Prospective sites along the Beutong section

The surface trace along the Beutong section is discontinuous along its 19-km length. The fault is formed by several fault strands that are separated by minor 0.6-0.8 km-wide step-overs (Hady, 2020; Marliyani and Hady, 2020). The main fault strand is mapped at the base of linear valley bounded by steep topography on both sides of the fault blocks with an average elevation of the topography on both sides of the fault about 950 meter above sea level (masl) A narrow linear valley along the fault trace captured most of the drainages from the hillslope, limiting our ability to identify any lateral offset along this section. Towards its southeastern end, we observed series of channels, with 600 m to 1.2 km spacing within 14.5 km distance, showing an apparent right lateral offset (sites 1-11, Figure 3). These channels are located along a secondary fault strand, which is located 16 km to the southwest from the main fault trace. Although apparent offset is visible, we cannot confidently match the channel heads to their respective channel tails at this location. Several channels may have formed at the same time and when they were moved by the fault, it might have created stream captures, which complicate the channel reconstruction effort. Beside the channel offsets, at this location we also identified several large ridges that show an apparent right lateral offset. Reconstruction of the top of these large ridges shows an apparent 2304 m right lateral offset. Although the offset of these ridge tops is measurable, dating them is challenging due to the lack of a flat surface associated with them, limiting their potential as paleoseismic sites.

3.2. Prospective sites along the Kuala Tripa section

The 15.7 km-long Kuala Tripa section is recognized as a narrow linear valley bordered on both sides by mountainous areas with average elevation of ~600 m asl. The morphology of the fault zone is characterized by a narrow valley with steep hillslopes, and a high drainage density on both sides. The fault trace consists of several fault strands, separated by 0.5-1 km wide step-overs. Along this section, we identified only four measurable offset channels with 297 m separation (sites 12-15, Figure 4). These observation points are located along the main fault trace, and they spread within 4 km distance. Most of the channels are flowing perpendicular to the fault; channels 13 and 14 are characterized by shutter ridge topography, providing plenty of piercing points and increasing their potentials for slip-rate studies.

3.3. Prospective sites along the Geumpang section

The Geumpang section spans a continuous length of 38.5 km. A fault discontinuity separates it from the Kuala Tripa Fault segment. Initially, for the first 20 km from its southeastern side, the fault is bordered by mountainous topography. Subsequently, for the next 18 km, a 3.8 km wide linear valley encloses the northeastern fault block. This configuration is conducive to the development of fault-perpendicular channels, with drainages flowing from the uplifted southwestern block to the northeastern block. Along this section, we identified 14 measurable offsets from 12 channels (sites 16-27). The observation points are clustered into three locations, with offsets varying in size from 12.6 to 323 m. The Geumpang section exhibits the largest number of small-sized offsets (<323 m) compared to other sections.

At site 27 (Figure 6), we acquired aerial photographs using a UAV drone and created a 15-cm resolution DEM. This new dataset enabled us to identify displacements at the meter scale. The smallest offset identified at this site measures 12.6 m. The fault at this location intersects Quaternary alluvium deposits, enhancing the potential for paleoseismic studies.

3.4. Prospective sites along the Mane section

The 18.8 km-length Mane section crosses mountainous area for half of its length, the second half toward its

northwestern end is bounded by a narrow (~1.3 km wide) valley. Along this section, we were only able to identify 5 measurable offsets from 5 channels (site 28-32, Figure 2). The offsets are ranging from 57 m to 351 m.

3.5. Prospective sites along the Jantho section

The Jantho section, spanning 33.6 km, traverses a mountainous area with elevations ranging from approximately 300 to 800 meters above sea level (asl). In this section, the fault exhibits minor discontinuities, including 0.2 to 2 km wide right and left step-overs, as well as fault branches. We conducted examinations at 10 sites along this section (sites 33-42, Figure 2 and 7) and identified 11 measurable offsets. The eleven channels are situated within a 8.5 km distance, with spacing ranging from 300 m to 1.3 km from each other. All these channels flow to the northeast, perpendicular to the fault. The offsets vary in size from 91 to 2332 m. Additionally, along this section, we observed an offset of approximately 2.3 km, similar to those found in the Beutong fault.

3.6. Prospective sites along the Indrapuri section

The Indrapuri section spans a total length of 28.9 km. In this section, the fault is discernible in the topography, marked by a distinct break in morphology between the mountainous range on the southwestern block and a vast alluvial plain on the northeastern side. The elevation difference between the alluvial plain and the mountain range is approximately 1200 meters above sea level (asl). Along this section, we identified 6 measurable offsets with size ranging from 111.113 to 858.27 m (sites 43-48, Figure 8-10).

3.7. Prospective sites along the Pulo Aceh section

The Pulo Aceh section, spanning a length of 50 km, mostly intersects the alluvial plain of Banda Aceh. The fault extends offshore along the northeastern boundary of the Pulo Aceh archipelago. However, along this section, we did not observe any measurable offset.

Discussions

We gathered a total of 35 data points over a distance of 200 kilometers along the Aceh Fault. The recognition of measurement sites is predominantly influenced not only by data resolution, but also by the geomorphological conditions along the fault zone. Additionally, not all displacements may be preserved in the landscape due to rainfall and climatic conditions that hinder the preservation of small-scale offsets.

Our data reveal that fault section with valley-bound topography, such as the Geumpang and Jantho faults, have more observation points than other faults bounded by mountainous topography on both sides, like the Beutong and Kuala Tripa faults. The topography bounded by mountains makes it challenging for a channel to maintain a linear shape and record lateral offset across the fault.

Some channels, such as those at sites 1-11 and 35-42, were evenly spaced with approximately 400-900 m intervals. The measurement at these channels was constrained by the channel spacing. As demonstrated and observed by several researchers (Reitman et al., 2019; Salisbury et al., 2018; Walker and Allen, 2012; Harbert et al., 2018), the downstream part of a channel is prone to detach from the head channel and may be captured by another nearby head channel, thereby obscuring the original offset. Because the large spacing, approximately 400-900 meters, between successive channels, theoretically allows us to avoid this head channel capture issue, we expected to observe more offsets in the range of a few meters to a couple of hundred meters. However, this is not evident in our observations.

We also observe that at sites where the channels are associated with shutter ridges, such as in sites 11, 14, 13, 21, 25, 35 and in 37-42, larger offsets are preserved (Figure 11). Plausible explanation is that the geomorphic configuration favoring the preservation of the offset as the surrounding landscape is protected by the shutter ridge, restraining the channel from cutting a new thalweg (Reitman et al., 2019; Harbert et al., 2018). The smallest identified offset is located along the Geumpang section (12.6 m, site 27, Figure 6). The local morphological configuration may vary from one drainage to another. However, our analysis of drainage patterns is conducted under the assumption that regional climate conditions are similar. Thus, the drainages have sustained comparable amounts of erosion and avulsion. The main difference between adjacent drainages is likely the local variation in geological formations, which may be more or less prone to erosion. For example, any suspicious offset data for a given drainage should be compared to the local geology to determine if the specific spot contains more erodible or stronger types of rock, ultimately influencing long-term morphological evolution.

Furthermore, the morphology of the drainage may also be influenced by local modifications of the river banks. In areas where the drainage crosses a fault, this can potentially lead to misinterpretations of the true offset and thus misinterpretations of the local slip rate. One effort to address this issue is to not rely solely on one offset marker. Instead, if available, multiple offset markers should be utilized to bracket the range of possible offsets and thus the slip rate. This approach has been successfully implemented in studying other fault systems (Yao et al., 2019).

Moreover, displacements along stream channels may not always indicate coseismic slip unless they are measured immediately after an earthquake (Reitman et al., 2019). Over time, these channels may undergo multiple geomorphic processes, such as erosion and aggradation. Additionally, the amount of fault slip may vary laterally along the rupture during an earthquake, depending on the fault geometry and subsurface lithological conditions (Reitman et al., 2019). As a result, clustered offset populations may reflect this variation and should be interpreted cautiously.

4. Conclusions

We documented the distribution of measurable lateral offsets along the Aceh Fault zone, identifying a total of 35 measurable offsets. The smallest identified offset is 12.6 m, while the maximum reached 2.3 km. Our data suggest that the tropical climatic conditions of Aceh as well as anthropic activity may have erased most of the recent fault displacements, preventing the preservation of offset markers over time. Additionally, our observations indicate that, aside from data resolution, the topographic setting—whether the fault is bounded by mountainous regions and/or valleys—may also impact the formation of observable lateral displacement.

Our offset measurements represent cumulative slip without constraints on their timing, making it challenging to estimate the fault slip rate. Since most of our observation points are along active channels, finding dateable material

Table 1. Result of the offset measurements

Site number	Figures	Types of Morphological features	Distance from NE-end (km)	Section	Calculated backslip (m)	Angle between the fault and channel (°)	Offset quality				Quality of geomorphic marker
							Geomorphic fault width (m)				
							A (north)	B (south)	Total	Rank	
6	3	channel	9.38	Beutong	301.38	75	157.5	147.3	304.8	3	high to low
9	3	channel	14.81	Beutong	301.38	83	245.9	227.3	473.2	3	high to low
12	4	channel	44.84	Kuala Tripa	296.58	54	64.9	112.2	177.1	2	moderate
13	4	channel	46.16	Kuala Tripa	296.58	54	73.9	270.4	344.3	3	moderate to low
14	4	channel	47.82	Kuala Tripa	296.58	87	151.8	136.2	288	3	high to low
15	4	channel	48.49	Kuala Tripa	296.58	57	34	54.7	88.7	1	moderate to high
16	apx	channel	65.91	Geumpang	100.43	68	97.4	41.1	138.5	1	high
18	apx	channel	68.54	Geumpang	100.43	69	123.8	161.4	285.2	3	high to low
19	apx	channel	72.32	Geumpang	184.24	84	66.9	106.2	173.1	1	high
20	apx	channel	72.93	Geumpang	184.24	79	51.4	239.1	290.5	3	high to low
21	apx	channel	73.17	Geumpang	184.24	71	51.4	239.1	290.5	3	high to low
22	apx	channel	73.94	Geumpang	184.24	59	61.3	42.9	104.2	1	moderate to high
23	apx	channel	74.19	Geumpang	184.24	76	77.9	40.9	118.8	1	high
24	apx	channel	74.72	Geumpang	184.24	62	139.8	79.8	219.6	2	high to moderate
25	apx	channel	74.92	Geumpang	184.24	58	139.8	79.8	219.6	2	moderate
26	5	channel	81.43	Geumpang	322.67	73	37.1	35.1	72.2	1	high
27	6	channel	86.32	Geumpang	102	51	44.1	102.7	146.8	1	moderate to high
27	6	channel	86.32	Geumpang	12.60	63	44.1	102.7	146.8	1	high
27	6	channel and linear ridge	86.32	Geumpang	48.40	60	44.1	102.7	146.8	1	high
28	apx	channel	99.47	Mane	57.37	72	128	175	303	3	high to low
29	apx	channel	100.27	Mane	274.3	67	102.1	96	198.1	2	high to moderate
30	apx	channel	102.06	Mane	425.11	78	90.8	124.4	215.2	2	high to moderate
31	apx	channel	110.75	Mane	236.77	66	11.9	43.5	55.4	1	high
32	apx	channel	113.57	Mane	351.23	88	120.5	98.1	218.6	2	high to moderate
33	apx	channel	134.32	Jantho	131.84	70	142.3	84.2	226.5	2	high to moderate
34	7	channel	136.63	Jantho	131.84	84	61	82.9	143.9	1	high
35	7	channel	137.94	Jantho	131.84	76	91	72.8	163.8	1	high
40	7	channel	141.63	Jantho	131.84	71	206.7	93.1	299.8	3	high to low
41	7, 8	channel	142.22	Jantho	91.48	70	91.5	70.8	162.3	1	high
41	7, 8	channel	142.22	Jantho	631.78	70	91.5	70.8	162.3	1	high
42	7, 8	channel	142.51	Jantho	430.01	65	91.5	112	203.5	2	high to moderate
44	9	channel	159.34	Indrapuri	472.89	77	106	71.9	177.9	2	high to moderate
46	9	channel	161.81	Pulo Aceh	472.89	60	130.5	44.6	175.1	1	high
47	9	paleochannel	184.37	Pulo Aceh	111.3	62	222	24	246	2	high to moderate
48	10	paleochannel	184.77	Pulo Aceh	111.3	42	50.8	25.6	76.4	1	high to moderate

Apx: appendix. Geomorphic fault width classification: (A) is distance of the piercing point to the fault on the northwestern block, (B) is distance of the piercing point to the fault on the southeastern block. Rank (1) narrow: < 176 m, (2) moderate: > 176 m, and (3) wide (3): > 279 m. The quality of geomorphic marker is in reference to its possibilities as slip-rate and paleoseismic sites.

might be difficult. Nevertheless, our study serves as a guide to locate prospective sites for detailed slip-rate studies, with priority given to areas with less complicated apparent offsets, such as in channels 19-25, 26, 27, 41, and 42.

Our study contributes additional evidence that the Aceh Fault is active, posing seismic hazards to the highly populated region along the fault, including the city of Banda Aceh. Furthermore, our research can be implemented toward a more detailed paleoseismic study supporting the development of maximum magnitude and earthquake recurrence models for the fault, crucial for seismic hazard analysis in the region. Considering the rapid landscape modifications in this environment, it is essential to document coseismic slip immediately after an earthquake. This condition is applicable not only in this region but also anywhere in Indonesia.

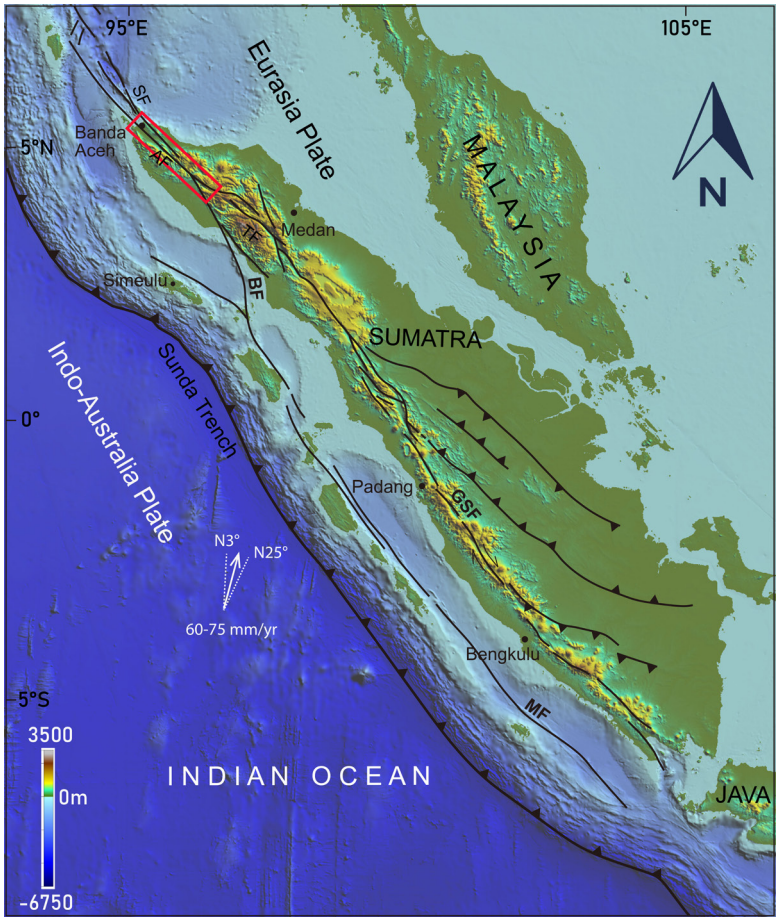

Figure 1. Tectonic setting of the Great Sumatran Fault (GSF) showing the map configuration of Aceh Fault (AF), Seulimeum Fault (SF), Mentawai Fault (MF), Tripa Fault (TF), and Batee Fault (BF). Red box delineates the location of our study. The outlined map and structural features are adapted and modified from Bellier and Sebrier (1995). The direction and velocity of convergence is adopted from DeMets et al., (1990) and McCaffrey (2000). Topography and bathymetric data is from The Global Multi-Resolution Topography (GMRT, freely available through https://www.gmrt.org/).

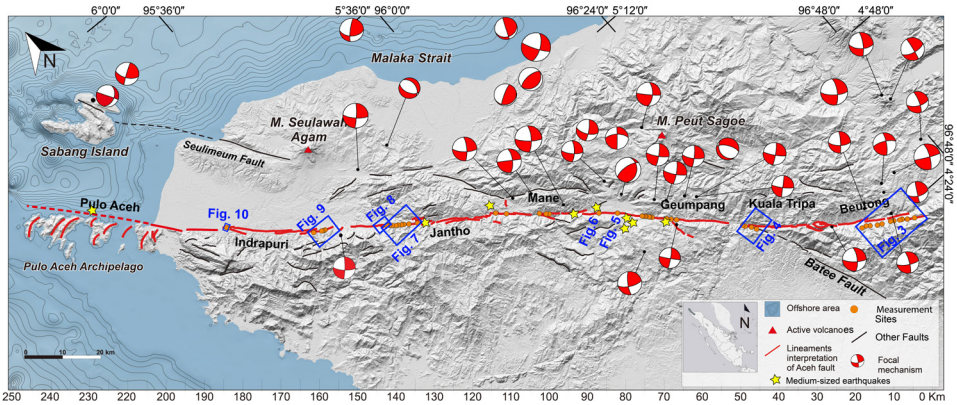

Figure 2. Map of the Aceh Fault zone and their associated earthquake focal mechanism. The focal mechanisms are from the GMT catalogue (https://www.globalcmt.org/CMTsearch.html). Yellow stars denote medium-sized (M4-5) earthquakes with no availability of focal mechanism information. The shaded relief map is from DEMNAS (http://tides.big.go.id/DEMNAS/DEMNAS.php). The bathymetry contour is from BATNAS data (http://tides.big.go.id/DEMNAS/Batnas.php). Blue boxes represent the locations of the subsequent figures of this paper.

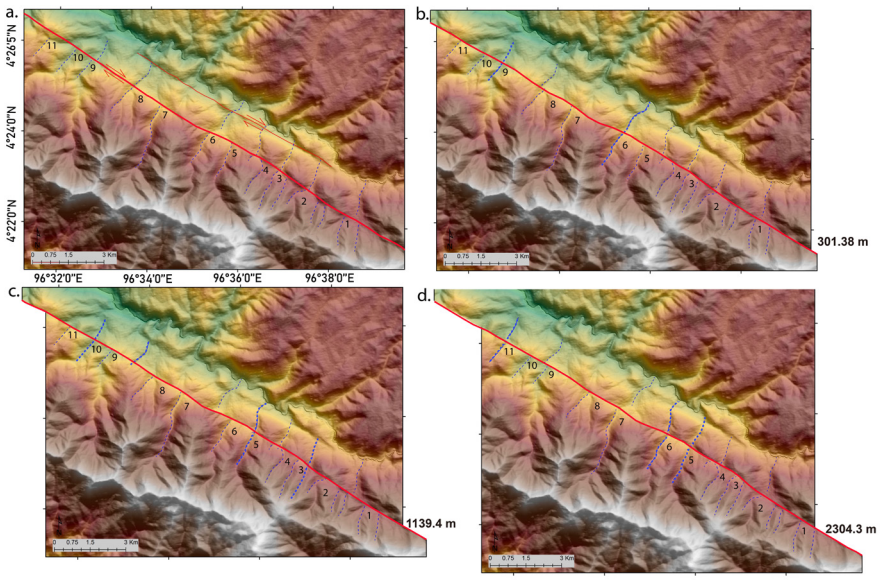

Figure 3. Successive reconstructions of offset channels from sites 1-11 along Beutong Fault (refer to Figure 2 for location). (a) map of the present configuration of the topography. Channels (blue dotted line) flows perpendicular to the fault plane (red line) and exhibit right lateral offset. (b-d) backslip reconstruction of the offset channel was done by retrofitting the channels into their initial alignment, yielding 301.38, 1139.4, and 2304.3m lateral offset. The realigned channel for each step is delineated as a thicker dashed blue line. The basemap is a hillshaded DEM from the DEMNAS data (https://tanahair.indonesia.go.id/demnas/#/). The channels (blue dotted lines) are labelled numerically from the southeastern end.

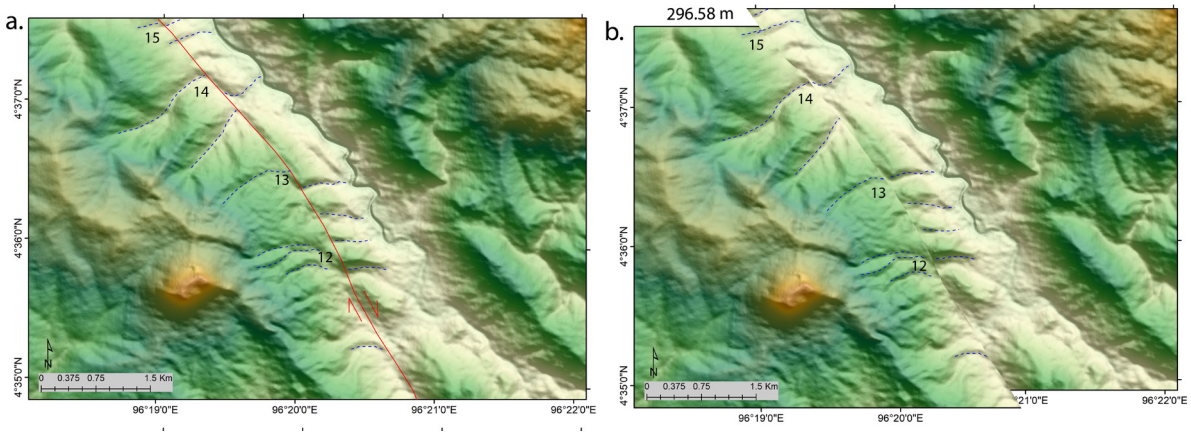

Figure 4. Successive reconstructions of offset channels from sites 12-15 along Kuala Tripa section (refer to Figure 2 for location). Most of the channels are flowing perpendicular to the fault; channels 13 and 14 are characterized by shutter ridge topography. (a) map of the present configuration of the topography, red line indicate Aceh Fault trace. (b) backslip reconstruction of the offset channel was done by retrofitting the channels (dotted black lines) into their initial aliignment, yielding 296.58 m lateral offset. The basemap is a hillshaded DEM from the DEMNAS data (https://tanahair.indonesia.go.id/demnas/#/).

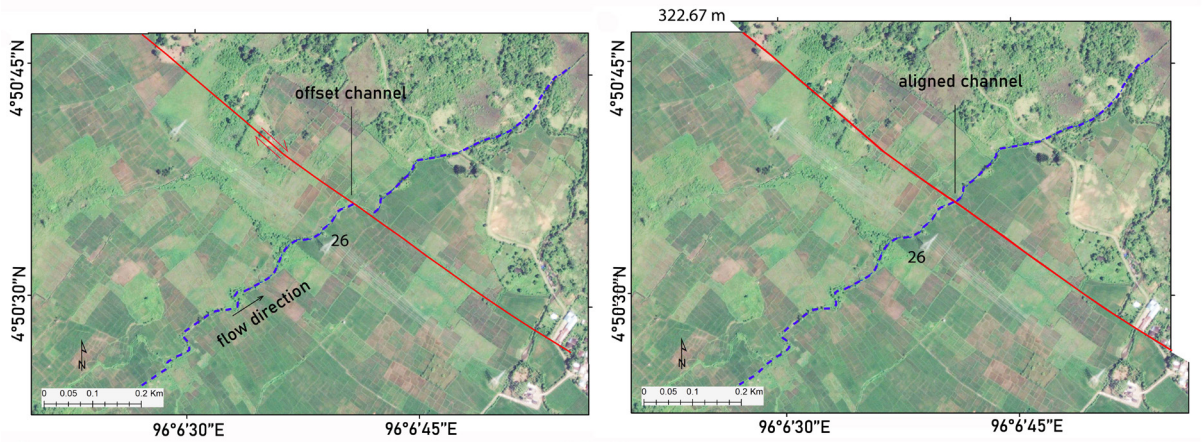

Figure 5. Backslip calculation at site 26 along Geumpang Fault section (refer to Figure 2 for location). Channel (blue dotted line) flows perpendicularly to the fault plane (red line) and offset laterally (right lateral). The measured offset is 322.67 m. The basemap is satellite imagery from Google Earth.

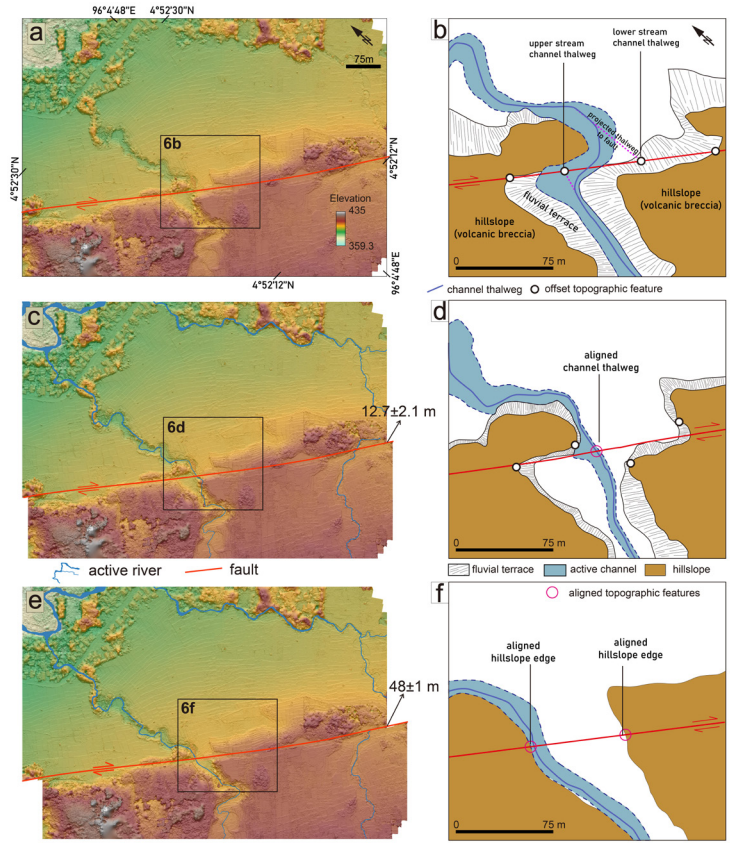

Figure 6. Successive back-slip reconstructions of a lateral offset channels at Geumpang fault at site 27. The base map is a DEM reconstructed using Structure from Motion procedure from UAV-based aerial photography (Bemis et al., 2013, 2014), the field data is adopted from Hady (2020) and Marliyani and Hady (2020). (a) DTM of area at km 89.5 (see Figure 2) where we observed a right lateral offset in a channel. (b) Interpreted geomorphology map, which illustrates the channel geometry in relation to the fault strand, serves as the foundation for uncertainty measurements. The projection line of the lower stream channel thalweg represents the maximum estimated distance. However, multiple possibilities exist due to the curvature in the flow direction of the channel. (c and d) Back calculation of the separation of the youngest channel thalweg resulted in a 12.7 displacement. (e and f) The back calculation of separation, based on hillslope morphology, resulted in a displacement of 48.4 meters.

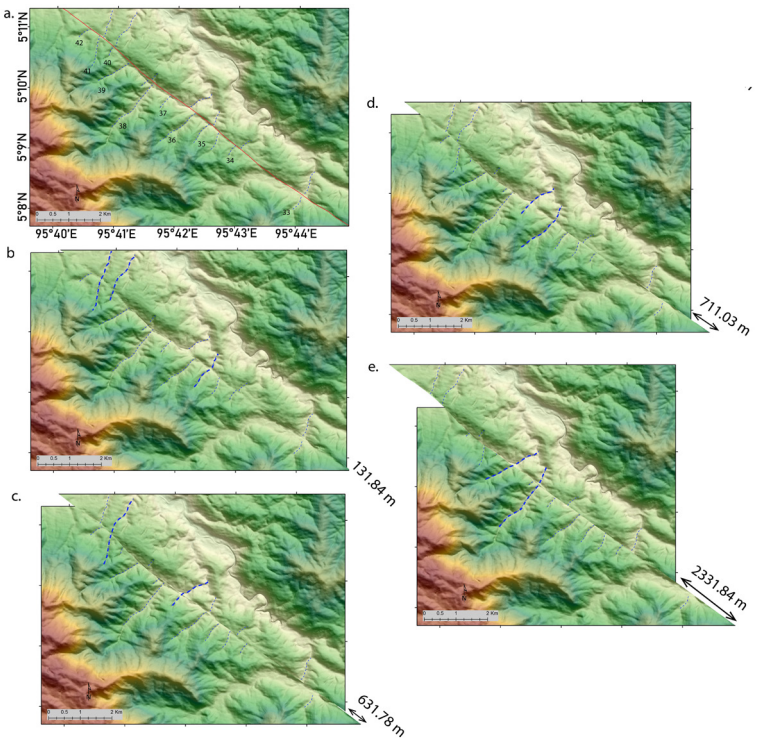

Figure 7. Backslip calculation at sites 34 - 42 along Jantho section (refer to Figure 2 for location). Channels (blue dotted line) flows perpendicular to the fault plane (red line) and exhibit right lateral offset. The measured offset is at 131.84, 631.78, 711.03, and 2331.84 m. The realigned channel for each step is delineated as a thicker dashed blue line. The basemap is a hillshaded DEM from the DEMNAS data (https://tanahair.indonesia.go.id/demnas/#/)

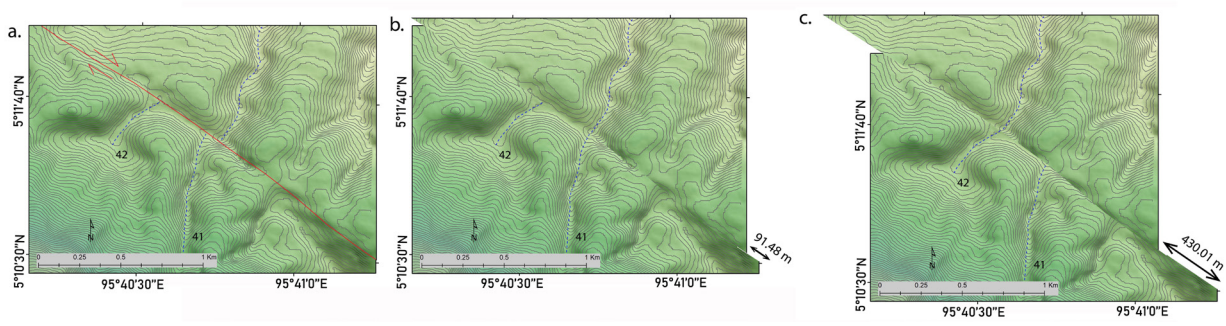

Figure 8. Backslip calculation at sites 41 and 42 along Jantho Fault section (refer to Figure 2 for location). Channels (blue dotted line) flows perpendicular to the fault plane (red line) and exhibit right lateral offset. The measured offset is at 91.48 and 430 m. The basemap is a hill shaded DEM from the DEMNAS data (https://tanahair.indonesia.go.id/demnas/#/)

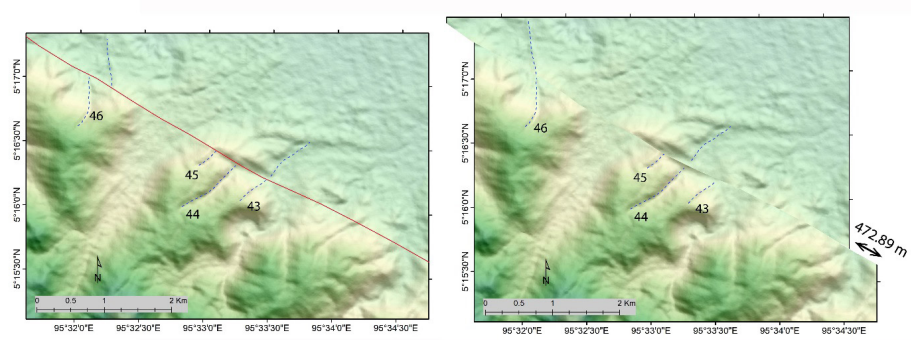

Figure 9. Backslip calculation at sites 43 and 46 along Indrapuri Fault section (refer to Figure 2 for location). Channels (blue dotted line) flows slightly oblique to the fault plane (red line) and exhibit right lateral offset. The measured offset is at 472.89 m. The basemap is a hill shaded DEM from the DEMNAS data (https://tanahair.indonesia.go.id/demnas/#/).

Figure 10. Backslip calculation at sites 47 and 48 along Indrapuri Fault section (refer to Figure 2 for location). We identified offset of several abandoned channels (black dotted lines). The paleochannel is typically filled with finer materials and is commonly utilized as a paddy field by the local community. We identified this channel by observing how people use the land for rice cultivation.vThe measured offset is at 111.3 m. The basemap is satellite imagery from Google Earth.

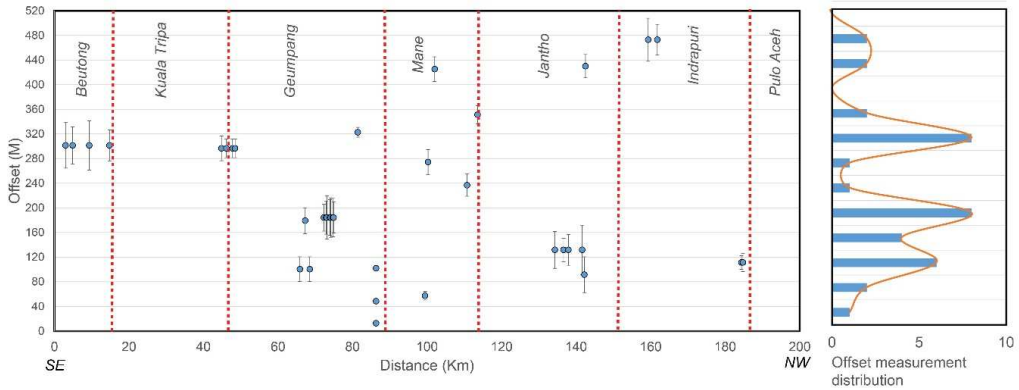

Figure 11. Right lateral offset measurements along the Aceh Fault zone by retrodeforming the geomorphic markers into their initial alignment. The uncertainties were determined based on the largest discrepancies between the preferred value and the accepted minimum or maximum value (see text for explanation). Figure on the right panel show a frequency lateral offset distribution. Dotted red lines indicate section boundaries.

Acknowledgement

This research was supported by funding from the France Indonesia Science and Technology Cooperation Program BOPTN SAME PHC NUSANTARA 2023 and partially supported by the funding from the Indonesian Meteorological and Geophysical Agency (BMKG).

References

Beaupretre, S., Garambois, S., Manighetti, I., Malavieille, J., Sénéchal, G., Chatton, M., Davies, T., Larroque, C., Rousset, D., Cotte, N. and Romano, C. (2012). Finding the buried record of past earthquakes with GPR-based palaeoseismology: a case study on the Hope fault, New Zealand. Geophysical Journal International, 189(1), 73-100.

Bennet, J.D., Mc Bridge, D., Cameron, N.R., Djunuddin, A., Ghazali, S.A., Jeffery, D.H., Kartawa, W., Keats, W., Rock, N.M.S., Thomson, S.J. and Whandoyo, R. (1981). Peta Geologi Lembar Banda Aceh, Sumatra (1: 250.000). Geologic Map of the Banda Aceh Quadrangle, Sumatra, Lembar (Quadrangle), 421, 19.

Curray, J. R., Moore, D. G., Lawver, L. A., Emmel, F. J., Raitt, R. W., Henry, M., & Kieckhefer, R. (1979). Tectonics of the Andaman Sea and Burma: convergent margins.

Diament, M., Harjono, H., Karta, K., Deplus, C., Dahrin, D., Zen Jr, M.T., Gerard, M., Lassal, O., Martin, A. and Malod, J. (1992). Mentawai fault zone off Sumatra: A new key to the geodynamics of western Indonesia. Geology, 20(3), 259-262.

DeMets, C., Gordon, R. G., Argus, D. F., & Stein, S. (1990). Current plate motions. Geophysical journal international, 101(2), 425-478.

De Pascale, G. P., Quigley, M. C., & Davies, T. R. (2014). Lidar reveals uniform Alpine fault offsets and bimodal plate boundary rupture behavior, New Zealand. Geology, 42(5), 411-414.

Bellier, O., & Sebrier, M. (1995). Is the slip rate variation on the Great Sumatran Fault accommodated by fore-arc stretching?. Geophysical Research Letters, 22(15), 1969-1972.

Bellier, O., Sebrier, M., Pramumijoyo, S., Beaudouin, T., Harjono, H., Bahar, I., & Forni, O. (1997). Paleoseismicity and seismic hazard along the Great Sumatran Fault (Indonesia). Journal of Geodynamics, 24(1-4), 169-183.

De Pascale, G. P., Quigley, M. C., & Davies, T. R. (2014). Lidar reveals uniform Alpine fault offsets and bimodal plate boundary rupture behavior, New Zealand. Geology, 42(5), 411-414.

Fitch, T. J. (1972). Plate convergence, transcurrent faults, and internal deformation adjacent to southeast Asia and the western Pacific. Journal of Geophysical research, 77(23), 4432-4460.

Hady, A. K. (2020). Geometri Dan Segmentasi Sesar Aceh (5.38 derajat N, 95.8 derajat E sampai 4.38 derajat N, 96.16 derajat E) Daerah Nagan Raya, Pidie, Dan Aceh Besar (Master thesis, Universitas Gadjah Mada).

Harbert, S. A., Duvall, A. R., & Tucker, G. E. (2018). The Role of Near-Fault Relief Elements in Creating and Maintaining a Strike-Slip Landscape. Geophysical Research Letters, 45(21), 11-683.

Genrich, J.F., Bock, Y., McCaffrey, R., Prawirodirdjo, L., Stevens, C.W., Puntodewo, S.S.O., Subarya, C. and Wdowinski, S. (2000). Distribution of slip at the northern Sumatran fault system. Journal of Geophysical Research: Solid Earth, 105(B12), 28327-28341.

Irsyam, M., Cummins, P.R., Asrurifak, M., Faizal, L., Natawidjaja, D.H., Widiyantoro, S., Meilano, I., Triyoso, W., Rudiyanto, A., Hidayati, S. and Ridwan, M., (2020). Development of the 2017 national seismic hazard maps of Indonesia. Earthquake Spectra, 36(1_suppl), pp.112-136.

Ito, T., Gunawan, E., Kimata, F., Tabei, T., Simons, M., Meilano, I., Ohta, Y., Nurdin, I. and Sugiyanto, D. (2012). Isolating along-strike variations in the depth extent of shallow creep and fault locking on the northern Great Sumatran Fault. Journal of Geophysical Research: Solid Earth, 117(B6).

Jarrard, R. D. (1986). Relations among subduction parameters. Reviews of Geophysics, 24(2), 217-284.

Jayangondaperumal, R., Thakur, V. C., Joevivek, V., Rao, P. S., & Gupta, A. K. (2018). Active Tectonics of Kumaun and Garhwal Himalaya. Springer Singapore.

Klinger, Y., Etchebes, M., Tapponnier, P., & Narteau, C. (2011). Characteristic slip for five great earthquakes along the Fuyun fault in China. Nature Geoscience, 4(6), 389-392.

Kondo, H., Awata, Y., Emre, O., Dogan, A., Ozalp, S., Tokay, F., Yıldırım, C., Yoshioka, T. and Okumura, K. (2005). Slip distribution, fault geometry, and fault segmentation of the 1944 Bolu-Gerede earthquake rupture, North Anatolian Fault, Turkey. Bulletin of the Seismological Society of America, 95(4), 1234-1249.

Langridge, R. M., Ries, W. F., Farrier, T., Barth, N. C., Khajavi, N., & De Pascale, G. P. (2014). Developing sub 5-m LiDAR DEMs for forested sections of the Alpine and Hope faults, South Island, New Zealand: Implications for structural interpretations. Journal of Structural Geology, 64, 53-66.

Lindvall, S. C., Rockwell, T. K., & Hudnut, K. W. (1989). Evidence for prehistoric earthquakes on the Superstition Hills fault from offset geomorphic features. Bulletin of the Seismological Society of America, 79(2), 342-361.

Hady, A. K., & Marliyani, G. I. (2020). Updated Segmentation Model of the Aceh Segment of the Great Sumatran Fault System in Northern Sumatra, Indonesia. Journal of Applied Geology, 5(2), 84-100.

McCaffrey, R. (1992). Oblique plate convergence, slip vectors, and forearc deformation. Journal of Geophysical Research: Solid Earth, 97(B6), 8905-8915.

McCaffrey, R. (2009). The tectonic framework of the Sumatran subduction zone. Annual Review of Earth and Planetary Sciences, 37, 345-366.

McCaffrey, R., Zwick, P.C., Bock, Y., Prawirodirdjo, L., Genrich, J.F., Stevens, C.W., Puntodewo, S.S.O. and Subarya, C., 2000. Strain partitioning during oblique plate convergence in northern Sumatra: Geodetic and seismologic constraints and numerical modeling. Journal of Geophysical Research: Solid Earth, 105(B12), pp.28363-28376.

McGill, S. F., & Sieh, K. (1991). Surficial offsets on the central and eastern Garlock fault associated with prehistoric earthquakes. Journal of Geophysical Research: Solid Earth, 96(B13), 21597-21621.

McGill, S. F., & Rubin, C. M. (1999). Surficial slip distribution on the central Emerson fault during the June 28, 1992, Landers earthquake, California. Journal of Geophysical Research: Solid Earth, 104(B3), 4811-4833.

Pusat Studi Gempa Nasional (2017). Peta Sumber dan Bahaya Gempa Tahun 2017. Bandung: Puslitbang Perumahan dan Permukiman Kementrian PUPR.

Reitman, N. G., Mueller, K. J., Tucker, G. E., Gold, R. D., Briggs, R. W., & Barnhart, K. R. (2019). Offset Channels May Not Accurately Record Strike-Slip Fault Displacement: Evidence From Landscape Evolution Models. Journal of Geophysical Research: Solid Earth, 124(12), 13427-13451.

Reitman, N. G., Klinger, Y., Briggs, R. W., & Gold, R. D. (2023). Climatic influence on the expression of strike-slip faulting. Geology, 51(1), 18-22.

Rockwell, T., Loughman, C., & Merifield, P. (1990). Late Quaternary rate of slip along the San Jacinto fault zone near Anza, southern California. Journal of Geophysical Research: Solid Earth, 95(B6), 8593-8605.

Salisbury, J. B., Rockwell, T. K., Middleton, T. J., & Hudnut, K. W. (2012). LiDAR and field observations of slip distribution for the most recent surface ruptures along the central San Jacinto fault. Bulletin of the Seismological Society of America, 102(2), 598-619.

Salisbury, J. B., Haddad, D. E., Rockwell, T., Arrowsmith, J. R., Madugo, C., Zielke, O., & Scharer, K. (2015). Validation of meter-scale surface faulting offset measurements from high-resolution topographic data. Geosphere, 11(6), 1884-1901.

Salisbury, J. B., Arrowsmith, J. R., Brown, N., Rockwell, T., Akciz, S., & Ludwig, L. G. (2018). The Age and Origin of Small Offsets at Van Matre Ranch along the San Andreas Fault in the Carrizo Plain, CaliforniaThe Age and Origin of Small Offsets at VMR along the SAF in the Carrizo Plain, California. Bulletin of the Seismological Society of America, 108(2), 639-653.

Sieh, K. E. (1978). Slip along the San Andreas fault associated with the great 1857 earthquake. Bulletin of the Seismological Society of America, 68(5), 1421-1448.

Sieh, K., & Natawidjaja, D. (2000). Neotectonics of the Sumatran fault, Indonesia. Journal of Geophysical Research, 105, 28,295–28,326. https://doi.org/10.1029/2000JB900120

Sieh, K., Zachariasen, J., Bock, Y., Edwards, L., Taylor, F., & Gans, P. (1994). Active tectonics of Sumatra. Geological Society of America Abstracts with Programs, 26, 382.

Singh, S. C., Moeremans, R., McArdle, J., & Johansen, K. (2013). Seismic images of the sliver strike-slip fault and back thrust in the Andaman-Nicobar region. Journal of Geophysical Research: Solid Earth, 118(10), 5208-5224.

Stirling, M., Gerstenberger, M., Litchfield, N., McVerry, G., Smith, W., Pettinga, J., & Barnes, P. (2008). Seismic hazard of the Canterbury region, New Zealand. Bulletin of the New Zealand Society for Earthquake Engineering, 41(2), 51-67.

Tabei, T., Kimata, F., Ito, T., Gunawan, E., Tsutsumi, H., Ohta, Y., Yamashina, T., Soeda, Y., Ismail, N., Nurdin, I. and Sugiyanto, D., (2017). Geodetic and geomorphic evaluations of earthquake generation potential of the northern Sumatran fault, Indonesia. In International Symposium on Geodesy for Earthquake and Natural Hazards (GENAH) Proceedings of the International Symposium on Geodesy for Earthquake and Natural Hazards (GENAH), Matsushima, Japan, 22-26 July, 2014 (pp. 21-28). Springer International Publishing.

Tong, X., Sandwell, D. T., & Schmidt, D. A. (2018). Surface creep rate and moment accumulation rate along the Aceh segment of the Sumatran fault from L-band ALOS-1/PALSAR-1 observations. Geophysical Research Letters, 45(8), 3404-3412.

Tregoning, P. (2002). Plate kinematics in the western Pacific derived from geodetic observations. Journal of Geophysical Research: Solid Earth, 107(B1), ECV-7.

Walker, F., & Allen, M. B. (2012). Offset rivers, drainage spacing and the record of strike-slip faulting: The Kuh Banan Fault, Iran. Tectonophysics, 530, 251-263.

Wells, D. L., & Coppersmith, K. J. (1994). New empirical relationships among magnitude, rupture length, rupture width, rupture area, and surface displacement. Bulletin of the seismological Society of America, 84(4), 974-1002.

Yao, W., Liu-Zeng, J., Oskin, M.E., Wang, W., Li, Z., Prush, V., Zhang, J., Shao, Y., Yuan, Z. and Klinger, Y. (2019). Reevaluation of the Late Pleistocene slip rate of the Haiyuan fault near Songshan, Gansu Province, China. Journal of Geophysical Research: Solid Earth, 124(5), pp.5217-5240.

Zielke, O., Arrowsmith, J. R., Ludwig, L. G., & Akçiz, S. O. (2010). Slip in the 1857 and earlier large earthquakes along the Carrizo Plain, San Andreas fault. Science, 327(5969), 1119-1122

Zielke, O., Klinger, Y. and Arrowsmith, J.R., (2015). Fault slip and earthquake recurrence along strike-slip faults—Contributions of high-resolution geomorphic data. Tectonophysics, 638, pp.43-62.